IN TER IM

OCIT

SWEPT-WING RECEPTIVITY STUDIES USING

DISTRIBUTED ROUGHNESS

Annual Technical Report
NAG 1 1925
ASU XAA0036

1A East Reid Street
Mail Stop 170
National Aeronautics and Space Administration
Langley Research Center
Hampton, Virginia 23681

Attention:
Ronald D. Joslin

January 1998

WILLIAM S. SARIC

Mechanical and Aerospace Engineering
College of Engineering and Applied Science
Arizona State University
Tempe, AZ 85287-6106

Janice D. Bennett, Director
Office of Research Creative Activity
(602) 965-8239

SWEPT-WING RECEPTIVITY STUDIES USING DISTRIBUTED ROUGHNESS

Mark S. Reibert[*]   William S. Saric[†]

Mechanical and Aerospace Engineering
Arizona State University
Tempe, Arizona 85287-6106

Abstract

This paper reviews the important recent progress in three-dimensional boundary-layer transition research. The review focuses on the crossflow instability that leads to transition on swept wings with a favorable pressure gradient. Following a brief overview of swept-wing instability mechanisms and the crossflow problem, a summary of the important findings of the 1990s is given. The discussion is presented from the experimental viewpoint, highlighting the ITAM work of Kachanov and co-workers, the DLR experiments of Bippes and co-workers, and the Arizona State University (ASU) investigations of Saric and co-workers. Where appropriate, relevant comparisons with CFD are drawn. The recent (last 18 months) research conducted by the ASU team is described in more detail in order to underscore the latest developments concerning nonlinear effects and transition control.

Nomenclature

A	disturbance amplitude
A_o	reference disturbance amplitude
C_p	pressure coefficient
C	airfoil streamwise chord (along X axis)
c	airfoil normal chord (along x axis)
f	frequency
k	roughness height

[*]Present address: Mystech Associates, 3233 E. Brookwood Court, Phoenix, AZ 85044. Member AIAA.
[†]Professor, Associate Fellow AIAA.

N $\quad = \ln(A/A_o)$, amplification factor

Re_c $\quad = U_\infty C/\nu$, chord Reynolds number

U $\quad = \left(u^2 + w^2\right)^{1/2}$, magnitude of total velocity, $U = U(y)$

U_e $\quad$ boundary-layer edge velocity along X axis

U_∞ $\quad$ freestream velocity along X axis

u, v, w $\quad$ velocity components in (X, Y, Z) coordinates

u', v', w' $\quad$ disturbance velocity in (X, Y, Z) coordinates

X, Y, Z $\quad$ global test-section coordinates: X is along the flow axis, Y is wall-normal, Z is unswept spanwise coordinate (positive down)

x, y, z $\quad$ model-oriented coordinates: x is chordwise, y is wall-normal, z is spanwise

α $\quad$ airfoil angle of attack

λ_s $\quad$ crossflow disturbance wavelength measured in swept span direction

ν $\quad$ kinematic viscosity

1 Introduction

1.1 Swept-Wing Flows

The study of three-dimensional boundary layers is motivated by the need to understand the fundamental instability mechanisms that cause transition in swept-wing flows. Research has identified four types of instabilities for these flows: attachment line, streamwise, centrifugal, and crossflow. The attachment-line problem is caused by a basic instability of the attachment-line boundary layer or by its contamination with turbulent disturbances and develops, in general, on swept wings with a large leading-edge radius (Poll 1979, 1984, 1985; Hall et al. 1984; Hall and Malik 1986). The streamwise instability is not unlike the familiar Tollmien-Schlichting (T-S) wave in two-dimensional flows. This mechanism is associated with the chordwise velocity component and is generally stabilized by a favorable pressure gradient. Centrifugal instabilities can appear over concave regions on the surface and result in the development of Görtler vortices (Floryan 1991; Benmalek and Saric 1994; Saric 1994). Crossflow waves, on the other hand, are an inviscid instability mechanism caused by the combined effect of wing sweep and pressure gradient. All of these instabilities can appear individually or together depending on the combination of Reynolds number, wall curvature, wing sweep, pressure gradient, and external disturbances. Thus, the swept wing provides a rich environment in which to study the stability behavior of three-dimensional boundary layers.

2

1.2 Crossflow Instability

The present review focuses on the crossflow instability that occurs on swept wings in regions of strong, favorable pressure gradient. Unlike T-S instabilities, the crossflow problem exhibits stationary ($f = 0$) as well as traveling disturbances that are amplified. Even though both types of waves are present in typical swept-wing flows, transition is usually dominated by either the stationary or the traveling waves. Linear theory predicts that the traveling disturbances are more highly amplified, however many experiments are dominated by stationary waves. Whether the stationary or traveling waves dominate is directly related to the receptivity process. Stationary waves dominate transition in low-disturbance environments, while traveling waves are more important in high-disturbance environments (Müller and Bippes 1989; Bippes 1990, 1991; Bippes 1991; Deyhle and Bippes 1996; Bippes 1997). Since the low-disturbance environment is more characteristic of flight, the stationary waves are expected to be more important.

Stationary crossflow waves (that is, the v' and w' disturbances) are typically very weak, hence analytical models have long been based on linear theory. However, experiments often show evidence of strong nonlinear effects (Dagenhart et al. 1989, 1990; Bippes and Nitschke-Kowsky 1990; Bippes et al. 1991; Deyhle et al. 1993; Reibert et al. 1996). The resolution of this apparent paradox lies in the understanding of the physical mechanism by which the stationary waves disturb the boundary layer. The key to the stationary disturbance is that the wave fronts are fixed with respect to the model and nearly aligned with the potential-flow direction (i.e., the wavenumber vector is nearly perpendicular to the inviscid streamline). Consequently, although the (v', w') motion of the wave is weak, its stationary nature produces an *integrated effect* that causes a strong u' distortion in the streamwise boundary-layer profile. This integrated effect and the resulting local distortion of the mean boundary layer leads to the modification of the basic state and the early development of nonlinear effects.

An interesting feature of the stationary crossflow waves is the destabilization of secondary instabilities. The u' distortions created by the stationary wave are time-independent, resulting in a spanwise modulation of the mean streamwise velocity profile. As the distortions grow, the boundary layer develops an alternating pattern of accelerated, decelerated, and doubly inflected profiles. The inflected profiles are inviscidly unstable and, as such, are subject to a high-frequency secondary instability (Kohama et al. 1991; Malik et al. 1994). This secondary instability is highly amplified and leads to rapid local breakdown. Because transition develops locally, the transition front is nonuniform in span and characterized by a "saw-tooth" pattern of turbulent wedges.

1.3 Literature Surveys

There is no shortage of publications in the field of boundary-layer stability and transition; certainly more than can be discussed in detail here. Comprehensive reviews for both two- and three-dimensional flows are given by Arnal (1984, 1986, 1992, 1994), Mack (1984), Poll (1984), Saric (1992b), and Reshotko (1994). Reed et al. (1996) give an up-to-date discussion of effectiveness and limitations of linear theory in describing boundary-layer instabilities. The reader is referred to these reports for overviews of much of the early work in stability and transition.

Several key papers provide in-depth reviews of stability and transition research in three-dimensional boundary layers and, in particular, swept-wing flows. Much of the early theoretical and experimental work is discussed by Reed and Saric (1989). Swept wings, rotating disks, axisymmetric bodies (rotating cones and spheres), corner flows, and attachment-line instabilities are reviewed, as well as the stability of flows for other three-dimensional geometries. This paper gives an excellent overview of the unique stability problems in three-dimensional flows. For swept wings, a historical account of the early investigations concerning the crossflow instability is given, along with a detailed literature survey.

1.4 Overview

Recently, improvements in both experimental techniques and computational methods have opened the door to a new understanding of transition in three-dimensional boundary layers. This paper will focus on the latest developments, with emphasis on the experimental work and relevant comparisons with CFD. In particular, the leading labs for three-dimensional boundary-layer research will be highlighted: Kachanov and co-workers at ITAM, Novosibirsk studying principally traveling crossflow waves; Bippes and co-workers at DLR, Göttingen investigating linear/nonlinear growth and the sensitivity to freestream conditions; Saric and co-workers at Arizona State University (ASU) focusing on the linear/nonlinear growth of stationary crossflow waves and the importance of surface-roughness-induced initial conditions. Both the ITAM and DLR work use a swept flat plate while the ASU model is a simulated infinite-span swept wing.

Bippes (1997) reviews the European contributions to stability and transition in three-dimensional boundary layers and as such is a companion paper to this work. In another paper, Kachanov (1996) reviews the efforts in ITAM, Novosibirsk. We therefore concentrate here on the U.S. efforts.

2 Summary of the Last Seven Years

Although crossflow disturbances have been observed experimentally since the early 1950s (Gray 1952), much of the important advances have occurred within this decade. The primary accomplishments are briefly summarized in the following paragraphs. A more detailed review of recent findings is given in section 3.

Micro-Thin Hot-Film Elements Multielement, microthin hot films developed at NASA Langley Research Center have been successfully used at ASU to obtain multipoint measurements in swept-wing flows (Dagenhart et al. 1989; Mangalam et al. 1990). The surface-mounted sensors can be distributed in the chordwise direction for multipoint monitoring of the transition location, or with the elements aligned along the stationary crossflow vortex axis for structure identification. The development of these gauges within a controlled transition experiment aided their implementation in the flight environment.

Secondary Instability In early experiments at ASU, Kohama et al. (1991) show that when the boundary layer is dominated by the stationary crossflow instability, transition is caused by a high-frequency secondary instability. This instability results from the local distortion of the mean streamwise boundary-layer profile by the stationary disturbance. As the stationary crossflow wave grows downstream, the *mean* boundary layer develops an alternating pattern of accelerated, decelerated, and doubly inflected profiles. The secondary instability develops locally as a result of the inviscidly unstable inflected profiles. The secondary instability is highly amplified, leading to rapid local breakdown and the characteristic "saw-tooth" transition front. Malik et al. (1994) put the idea on firm footing with an analysis of the secondary instability and obtained agreement with Kohama et al. (1991).

Linear Growth In the earlier work of Nitschke-Kowsky and Bippes (1988), Müller (1990), Deyhle et al. (1993), Kachanov and Tararykin (1990), and Kachanov (1996), the observed wavelength and growth rate of the crossflow wave is initially in general agreement with linear theory and is independent of the freestream turbulence level. However, it is reported that superposing a spanwise periodicity on the flow fixes the wavelength of the stationary disturbance.

Forced Traveling Modes Deyhle et al. (1993) and Kachanov (1996) develop techniques to create controlled traveling waves within the boundary layer and observe the growth of traveling modes. Linear theory was verified in this case. The importance of traveling modes and their dependence on freestream conditions and are put into perspective by Bippes (1997).

Sensitivity to Freestream Conditions The DLR experiments of Bippes and co-workers provide important results concerning the role of freestream disturbances. The primary findings are reported by Nitschke-Kowsky and Bippes (1988), Müller and Bippes (1989), Bippes (1990, 1991), Bippes and Müller (1990), Bippes and Nitschke-Kowsky (1990), Müller (1990), Müller et al. (1990), and Bippes et al. (1991). Recent results are summarized by Deyhle et al. (1993), Lerche and Bippes (1995), Deyhle and Bippes (1996), and Bippes (1997). These experiments measure both stationary and traveling crossflow waves, however their relative importance in influencing the details of transition is found to depend on the freestream turbulence level. Müller and Bippes (1989) describe a series of comparative experiments using the same swept flat plate in both low- and high-turbulence tunnels. The stationary waves are found to dominate transition in the low-disturbance environment, however in the high-turbulence tunnel both the growth rate and final amplitude of the stationary disturbance are reduced. At the same time, the traveling waves show larger growth rates and dominate transition.

Not only does the type of transition depend on freestream conditions, but Deyhle and Bippes (1996) show that transition can be initially delayed by *increasing* the freestream turbulence levels. In this case, the strong stationary modes are not as effective in causing the secondary instability because of the unsteadiness in the boundary layer.

Sensitivity to Roughness At ONERA-CERT, Arnal et al. (1990) use isolated roughness to verify the roughness correlation of von Doenhoff and Braslow (1961). This involves using roughness elements as a bypass, i.e., transition occurs just downstream of the roughness element.

In the DLR experiments, Müller and Bippes (1989) show that the stationary waves remain fixed with respect to the model regardless of the wind tunnel in which the experiment is conducted. This indicates that the stationary crossflow instability is sensitive to initial conditions provided by surface roughness.

In work reported by Radeztsky et al. (1993), the ASU team investigated the sensitivity of stationary cross-flow waves to roughness-induced initial conditions by introducing isolated, micron-sized, artificial roughness elements near the leading edge. These experiments show that a single, three-dimensional roughness element can locally amplify the stationary wave leading to premature transition behind the roughness element. Only single roughness elements are used in these tests, and the effects on transition are observed to occur only in the region downstream of the roughness element. Moreover, the roughness element causes early transition only when its diameter is larger than 10% of the most-unstable-mode wavelength and is placed near Branch I of the stationary instability.

Nonlinear Saturation In all the DLR experiments, the growth of the stationary and traveling crossflow waves shows initial qualitative agreement with linear theory. However, the disturbance amplitude saturates due to nonlinear effects. Also, the amplitude of the traveling waves shows a spanwise modulation indicating nonlinear interactions with the stationary modes.

In experiments at ASU, Reibert et al. (1995, 1996) investigate the nonlinear saturation of stationary waves using micron-sized artificial roughness elements to control the initial conditions. Full-span arrays of roughness elements are used to preserve the spanwise periodicity of the disturbance. By forcing the most unstable mode (according to linear theory), nonlinear saturation of the disturbance amplitude is observed well before transition. Although the initial growth rate increases with increasing roughness height, the saturation *amplitude* remains largely unaffected by changes in the roughness height.

The presence of a large laminar extent of nonlinear saturation gives rise to a certain difficulty in using linear methods—such as e^N or linear PSE—to predict transition. The futility of such approaches is expressed by Arnal (1994) and Reed et al. (1996), who show that linear methods do not work in three-dimensional boundary layers.

Modal Decomposition Radeztsky et al. (1994) describe a measurement technique that allows the experimentally obtained stationary crossflow structure to be decomposed into its spatial modes. Using a high-resolution traversing mechanism, hot wires are carefully moved through the boundary layer along a predetermined path. Data are acquired at numerous spanwise locations, from which modal information is extracted using a spatial power spectrum. Reibert et al. (1996) use a slightly modified technique to more objectively determine the modal content. Under certain conditions, the amplitude of the fundamental disturbance mode plus eight harmonics are successfully extracted from the experimental data.

Excitation of Less Unstable Modes Using the modal decomposition technique described above, Reibert et al. (1996) investigate the effect of roughness-induced forcing at a wavelength three times that of the most unstable stationary mode (according to linear theory). A cascading of energy from the fundamental to higher modes (smaller wavelengths) is observed, leading to nonlinear interactions among the fundamental mode and its harmonics. Transition is observed to occur slightly earlier compared to forcing at the most unstable wavelength, and the saw-tooth transition front is much more "regular" in span. These data indicate that nonlinear interactions among multiple modes is important in determining the details of transition.

Excitation of Subcritical Modes Continuing the experiments of Reibert et al. (1996), Carrillo (1996) describes a set of experiments in which the stationary crossflow disturbance is forced with subcritical roughness spacing, i.e., the spacing between roughness elements is less than the wavelength of the mode unstable mode. Under these conditions, the rapid growth of the forced mode completely suppresses the linearly most unstable mode, thereby delaying transition beyond its "natural" location (i.e., where transition occurs in the absence of artificial roughness). These data demonstrate that surface roughness can be used to *control* the stationary crossflow disturbance wavenumber spectrum in order to delay transition on swept wings.

Structure Identification Using POD Using data collected at ASU, Chapman et al. (1995, 1996) apply linear stochastic estimation (LSE) and proper orthogonal decomposition (POD) to identify the spatio-temporal evolution of structures within a swept-wing boundary layer. Detailed measurements are acquired using multielement hot-film, hot-wire, and cross-wire anemometry. These data allow the POD to objectively determine (based on energy) the modes characteristic of the measured flow. Data are acquired through the transition region, from which an *objective* transition-detection method is developed using the streamwise spatial POD solutions.

CFD Comparisons (DNS) Direct numerical simulations (DNS) have historically been constrained by computer resources and algorithmic limitations, however some successes have been achieved in relation to the stationary crossflow problem. Reed and Lin (1987) and Lin (1992) perform DNS for stationary waves on an infinite-span swept wing similar to the ASU experiments. Meyer and Kleiser (1990) investigate the disturbance interactions between stationary and traveling crossflow modes on a swept flat plate using Falkner-Scan-Cooke similarity profiles for the basic state. The results are compared to the experiments of Müller and Bippes (1989). With an appropriate initial disturbance field, the nonlinear development of stationary and traveling crossflow modes is simulated reasonably well up to transition. Wintergerste and Kleiser (1995) continue this work by using DNS to investigate the breakdown of crossflow vortices in the highly nonlinear final stages of transition.

CFD Comparisons (PSE) Combining the ability to include nonparallel and nonlinear effects with computationally efficient parabolic marching algorithms, the parabolized stability equations (PSE) developed by Herbert (1994) have recently been used to successfully model the crossflow instability. For swept-wing flows, nonlinear PSE calculations exhibit the disturbance amplitude saturation characteristic of the DLR and ASU experiments. Wang et al. (1994) investigate both stationary and traveling crossflow waves for the

8

swept airfoil used in the ASU experiments and predict nonlinear amplitude saturation for both types of disturbances. It is suggested that the interaction between the stationary and traveling waves is an important aspect of the transition process.

Within the last year, the PSE have been used at ASU to model the growth and development of the stationary crossflow wave with remarkable precision. Using the experimental data of Reibert (1996) to guide the initial conditions, Haynes and Reed (1996) are able to accurately predict the nonlinear amplitude saturation and model the detailed structure and evolution of the stationary crossflow wave. An interesting discovery of Haynes (1996) is a hyper-sensitivity to seemingly negligible streamline and body curvature in the ASU experiments.

3   Recent Results

The preceding section briefly summarizes the important findings of the 1990s and lays the foundation for understanding the current state of knowledge related to the crossflow instability. Building on that foundation, this section presents a more detailed review of the last 18 months. In the interest of brevity, the focus will shift exclusively to the ASU experiments of Saric and co-workers and computations of Reed and co-workers. The reader is referred to Bippes (1997) for a more detailed review of recent DLR and other European work.

3.1   The ASU Experiment

The ASU crossflow experiments are conducted in the Arizona State University Unsteady Wind Tunnel—a low-speed, low-turbulence, closed-circuit facility in which the stability and transition of laminar boundary layers are studied (Saric 1992a). The NLF(2)-0415 airfoil model (Somers and Horstmann 1985) is mounted vertically in the 1.4 m × 1.4 m × 4.9 m test section. Floor and ceiling contours installed in the test section produce an infinite-span swept-wing flow (figure 1). With a 45° sweep and a −4° angle of attack, the favorable pressure gradient produces considerable crossflow while suppressing T-S modes (figure 2).

The aluminum surface of the NLF(2)-0415 is hand polished to a 0.25 μm rms finish so that even micron-sized artificial roughness elements are well above the background roughness level. Detailed hot-wire measurements within the boundary layer provide two-dimensional maps of the stationary disturbance structure, while spectral techniques are used to identify and follow specific stationary modes.

3.2 Nonlinear Interaction and Amplitude Saturation

3.2.1 Natural Roughness

In the absence of artificial surface roughness, the naturally occurring stationary crossflow waves are nonuniform in span due to submicron surface irregularities near the leading edge. This is shown in figure 3, which displays a contour plot of the normalized boundary-layer velocity at $x/c = 0.45$ for $Re_c = 3.0 \times 10^6$. The figure shows the streamwise velocity u/U_e in the (Y, z) plane. The flow is toward the reader (i.e., the observer is looking upstream into the oncoming boundary-layer flow), and the stationary vortices are turning in the right-handed sense. The velocity contours are constructed from 100 mean-flow boundary-layer profiles each separated by 1 mm in span. It is important to note that the wave-like structure of figure 3 represents the integrated effect of the weak stationary vortices on the streamwise velocity.

Figure 3 displays a dominant feature at a 12 mm spanwise spacing, which is approximately the most amplified stationary wavelength according to linear theory. At the same time, the richness in the spectral content is evident and indicates nonlinear interaction among many modes. This is typical of all the early experiments (Müller and Bippes 1989; Dagenhart et al. 1989, 1990; Bippes and Nitschke-Kowsky 1990; Bippes et al. 1991).

3.2.2 Critical Forcing

The initial conditions are controlled by applying a full-span array of $k = 6$ μm roughness elements at $x/c = 0.023$. The spanwise spacing of the elements is 12 mm, corresponding to the naturally occurring most-amplified wavelength. Figure 4 shows the streamwise velocity contour with the roughness installed. The dominance of the 12 mm mode is striking, and allows a direct calculation of the stationary disturbance amplitude (see Reibert et al. 1996 for a description of the technique).

Figure 5 compares the experimental amplification factor ("N-factor") for the 12 mm roughness forcing with the predictions of the Orr-Sommerfeld equation (OSE), the linear parabolized stability equations, and the full nonlinear parabolized stability equations. All computational results are provided by Haynes (1996). The saturation phenomenon is clearly evident, and can be quantified. The early growth shows excellent agreement with linear PSE, however strong nonlinear effects develop well before transition at $(x/c)_{tr} = 0.52$. The importance of nonparallel effects is indicated by the failure of traditional linear stability theory (OSE) to accurately predict the growth even in the linear range. When nonlinearity is added, the agreement is remarkable over the entire measurement region and all aspects of the growth are predicted. This is explained

in more detail in Reibert et al. (1996), Reibert (1996), and Haynes (1996).

The outstanding agreement shown in figure 5 results from the inclusion of curvature in the computations, without which the disturbance growth is significantly overpredicted. The sensitivity to very weak curvature is due to the strong stabilizing Görtler effect with convex curvature (Benmalek and Saric 1994). This is the reason for the disagreement between the linear experiments of Radeztsky et al. (1994) and linear theory without curvature. More information on the sensitivity to curvature can be found in Haynes (1996).

3.2.3 Multiple-Mode Crossflow Waves

Multiple-mode crossflow waves are produced by increasing the space between the roughness elements. Figure 6 shows the streamwise velocity contour obtained with a roughness spacing of 36 mm. The primary structures are 36 mm apart corresponding to the roughness spacing. In addition, superharmonics are present at integer multiples of the primary wavenumber. This is clearly indicated by the power spectral density (PSD) plotted in figure 7, which displays amplified modes with wavelengths of 36 mm, 18 mm, 12 mm, 9 mm, 7.2 mm, 6 mm, 5.1 mm, 4.5 mm, and 4 mm. The presence of this roughness-induced harmonic sequence indicates that the stationary crossflow pattern is not predetermined by external flow conditions, but can be completely controlled by the surface characteristics.

3.3 Distributed Roughness and the Importance of Spanwise Spacing

Two important observations concerning the long-wavelength ($\lambda_s = 36$ mm) data of Reibert et al. (1996) are:

1. Unstable waves occur only at integer multiples of the primary disturbance wavenumber, and

2. No subharmonic disturbances are destabilized.

In other words, spacing the roughness elements 36 mm apart excites disturbances with spanwise wavelengths of 36 mm, 18 mm, 12 mm, 9 mm, etc., but does not produce any unstable waves with "intermediate" wavelengths or with wavelengths greater than 36 mm.

Following this lead, the Carrillo (1996) investigates the effects of distributed roughness whose primary disturbance wavenumber does not contain a harmonic at $\lambda_s = 12$ mm (the most unstable wavelength according to linear theory).

11

3.3.1 Noncritical Forcing

The harmonic nature of the roughness-induced stationary crossflow disturbance is confirmed by changing the fundamental disturbance wavelength (i.e., the roughness spacing) to 18 mm. Figure 8 shows the streamwise velocity contours at $x/c = 0.45$ and $Re_c = 2.4 \times 10^6$ for this configuration. The corresponding PSD is shown in figure 9.

The velocity contours clearly show the presence of the 18 mm and 9 mm wavelength, and the PSD confirms that the 18 mm forcing has produced the sequence of harmonics at $\lambda_s = 18$ mm, 9 mm, 6 mm, etc. The most important feature of figure 9, however, is that *the linearly most unstable disturbance ($\lambda_s = 12$ mm) has been completely suppressed*. Moreover (and consistent with all previous results), no subharmonic disturbances are observed.

3.3.2 Subcritical Forcing

The 18 mm forcing case proves that an appropriately designed roughness configuration can, in fact, inhibit the growth of the (naturally occurring) most-unstable disturbance. Unfortunately, the transition location remains relatively unchanged due to the nonlinear interaction between the $\lambda_s = 18$ mm and the $\lambda_s = 9$ mm modes.

The disturbance field changes remarkably, however, when the roughness spacing is reduced to inhibit the growth of all disturbances whose wavelength is greater than that of the linearly most unstable disturbance. Figures 10 and 11 show the streamwise velocity contours for 8 mm spaced roughness at $x/c = 0.30$ and $x/c = 0.60$, respectively. The corresponding PSD are shown in figures 12 and 13. These data clearly indicate that the disturbance is initially dominated by the $\lambda_s = 8$ mm mode, yet transforms to a "broad-band" disturbance downstream.

The broad-band nature of the disturbance for large x/c (figure 13) indicates that the long-wavelength disturbances are not subharmonics of the fundamental ($\lambda_s = 8$ mm) instability. Instead, this indicates broad-band growth of the "background" disturbances, which are only observed once the otherwise dominating fundamental mode decays. This is clearly indicated in figure 14, which compares the total disturbance amplitude to that of the $\lambda_s = 8$ mm mode as a function of chord position. As the $\lambda_s = 8$ mm mode decays for $x/c \geq 0.30$, the long-wavelength, broad-band disturbances become unstable so that the total disturbance energy increases for $x/c \geq 0.50$.

3.3.3 Transition Location

The most remarkable result obtained from the subcritical roughness spacing is the dramatic affect on transition location. In the absence of artificial roughness, transition occurs near the pressure minimum at $x/c = 0.71$ for $Re_c = 2.4 \times 10^6$. Adding $k = 6\,\mu m$ roughness with a spanwise spacing equal to (or a multiple of) the wavelength of the linearly most unstable wave ($\lambda_s = 12$ mm) moves transition forward to $x/c \leq 0.52$. However, the subcritical forcing at 8 mm spanwise spacing actually *delays transition beyond the pressure minimum and onto the trailing-edge flap at* $x/c = 0.80$.

4 Conclusions

Boundary-layer transition in three-dimensional flows is a complicated process involving complex geometries, multiple instability mechanisms, and nonlinear interactions. Yet significant progress has been recently made toward understanding the stability and transition characteristics of swept-wing flows. Concerning the crossflow problem, the past seven years have produced several important discoveries including:

- Development of instrumentation that can be applied to the flight-test environment.

- Application of POD methods to interpret wind-tunnel and flight-test transition data.

- Effect of environmental conditions in determining the relative importance of stationary and traveling waves.

- Existence of a secondary instability causing local transition in stationary-crossflow-dominated flows.

- Sensitivity of the stationary disturbance to leading-edge surface roughness.

- Importance of nonlinear effects and modal interaction.

- Development of nonlinear PSE codes to predict all aspects of stationary disturbance growth.

- Sensitivity of stationary wave growth to very weak convex curvature.

- Use of artificial roughness to control the disturbance wavenumber spectrum and delay transition.

Three-dimensional boundary-layer stability is still far from being completely explained. Important factors such as receptivity—the process by which external disturbances enter the boundary layer and create the initial conditions for an instability—are still not well understood. Yet in spite of these shortcomings, careful

experiments and accurate computations have resulted in significant progress toward understanding a difficult problem.

Acknowledgments

References

Arnal, D. 1984. Description and prediction of transition in two-dimensional incompressible flow. In *Special Course on Stability and Transition of Laminar Flows*, AGARD R-709.

Arnal, D. 1986. Three-dimensional boundary layers: Laminar-turbulent transition. In *Special Course on Calculation of Three-Dimensional Boundary Layers with Separation*, AGARD R-741.

Arnal, D. 1992. Boundary-layer transition: Prediction, application to drag reduction. In *Special Course on Skin Friction Drag Reduction*, AGARD R-786. Loughton, Essex: Specialised Printing Services Ltd. ISBN 92-835-0661-8.

Arnal, D. 1994. Boundary-layer transition: Predictions based on linear theory. In *Special Course on Progress in Transition Modelling*, AGARD R-793. Loughton, Essex: Specialised Printing Services Ltd. ISBN 92-835-0742-8.

Arnal, D., G. Casalis, and J. C. Juillen. 1990. Experimental and theoretical analysis of natural transition on infinite swept wing. In *Laminar-Turbulent Transition* (eds. D. Arnal and R. Michel), vol. 3, pp. 311–325. Berlin: Springer-Verlag. ISBN 3-540-52196-8.

Benmalek, A. and W. S. Saric. 1994. Effects of curvature variations on the nonlinear evolution of Goertler vortices. *Phys. Fluids* 3(10):3353–3367.

Bippes, H. 1990. Instability feature appearing on swept wing configurations. In *Laminar-Turbulent Transition* (eds. D. Arnal and R. Michel), vol. 3, pp. 419–430. Berlin: Springer-Verlag. ISBN 3-540-52196-8.

Bippes, H. 1991. Experiments on transition in three-dimensional accelerated boundary-layer flows. In *Proc. R.A.S. Boundary Layer Transition and Control*, Cambridge, U.K.

Bippes, H. 1997. Environmental conditions and transition prediction in 3-D boundary layers. AIAA Paper 97-1906.

Bippes, H. and B. Müller. 1990. Disturbance growth in an unstable three-dimensional boundary layer. In *Numerical and Physical Aspects of Aerodynamics Flows IV* (ed. T. Cebeci), pp. 345-358. Berlin: Springer-Verlag. ISBN 3-540-52259-X.

Bippes, H. and P. Nitschke-Kowsky. 1990. Experimental study of instability modes in a three-dimensional boundary layer. *AIAA J.* 28(10):1758-1763.

Bippes, H., B. Müller, and M. Wagner. 1991. Measurements and stability calculations of the disturbance growth in an unstable three-dimensional boundary layer. *Phys. Fluids* 3(10):2371-2377.

Carrillo, R. B. Jr. 1996. *Distributed-Roughness Effects on Stability and Transition in Swept-Wing Boundary Layers.* Master's thesis, Arizona State University.

Chapman, K. L., M. N. Glauser, M. S. Reibert, and W. S. Saric. 1995. Proper orthogonal decomposition applied to boundary-layer transition on a swept wing. In *Transitional Boundary Layers in Aeronautics* (eds. R. A. W. M. Henkes and J. L. van Ingen), pp. 165-173. Amsterdam. North-Holland Press. ISBN 0-444-85812-1.

Chapman, K. L., M. N. Glauser, M. S. Reibert, and W. S. Saric. 1996. A multi-point correlation analysis of a crossflow-dominated boundary layer. AIAA Paper 96-0186.

Dagenhart, J. R., W. S. Saric, M. C. Mousseux, and J. P. Stack. 1989. Crossflow vortex instability and transition on a 45-degree swept wing. AIAA Paper 89-1892.

Dagenhart, J. R., W. S. Saric, J. A. Hoos, and M. C. Mousseux. 1990. Experiments on swept-wing boundary layers. In *Laminar-Turbulent Transition* (eds. D. Arnal and R. Michel), vol. 3, pp. 369-380. Berlin: Springer-Verlag. ISBN 3-540-52196-8.

Deyhle, H. and H. Bippes. 1996. Disturbance growth in an unstable three-dimensional boundary layer and its dependence on environmental conditions. *J. Fluid Mech.* 316:73-113.

Deyhle, H., G. Höhler, and H. Bippes. 1993. Experimental investigation of instability wave propagation in a 3-D boundary-layer flow. *AIAA J.* 31(4):637-645.

Floryan, J. M. 1991. On the Görtler instability of boundary layers. *Prog. Aerospace Sci.* 28:235-271.

Gray, W. E. 1952. The effect of wing sweep on laminar flow. RAE TM Aero 255.

Hall, P. and M. R. Malik. 1986. On the instability of a three-dimensional attachment-line boundary layer: Weakly nonlinear theory and a numerical approach. *J. Fluid Mech.* 163:257–282.

Hall, P., M. R. Malik, and D. I. A. Poll. 1984. On the stability of an infinite swept attachment-line boundary layer. *Phil. Trans. Roy. Soc. Lon. A* 395:229–245.

Haynes, T. S. 1996. *Nonlinear Stability and Saturation of Crossflow Vortices in Swept-Wing Boundary Layers.* Ph.D. diss., Arizona State University.

Haynes, T. S. and H. L. Reed. 1996. Computations in nonlinear saturation of stationary crossflow vortices in a swept-wing boundary layer. AIAA Paper 96-0182.

Herbert, T. 1994. Parabolized stability equations. In *Special Course on Progress in Transition Modelling*, AGARD R-793. Loughton, Essex: Specialised Printing Services Ltd. ISBN 92-835-0742-8.

Kachanov, Y. S. 1996. Experimental studies of three-dimensional instability of boundary layers. AIAA Paper 96-1976.

Kachanov, Y. S. and O. I. Tararykin. 1990. The experimental investigation of stability and receptivity of a swept-wing flow. In *Laminar-Turbulent Transition* (eds. D. Arnal and R. Michel), vol. 3, pp. 499–509. Berlin: Springer-Verlag. ISBN 3-540-52196-8.

Kohama, Y., W. S. Saric, and J. A. Hoos. 1991. A high-frequency secondary instability of crossflow vortices that leads to transition. In *Proc. R.A.S. Boundary Layer Transition and Control*, Cambridge, U.K.

Lerche, T. and H. Bippes. 1995. Experimental investigation of cross-flow instability under the influence of controlled disturbance excitation. In *Transitional Boundary Layers in Aeronautics* (eds. R. A. W. M. Henkes and J. L. van Ingen), pp. 137–144, Amsterdam. North-Holland Press. ISBN 0-444-85812-1.

Lin. R.-S. 1992. *Stationary Crossflow Instability on an Infinite Swept Wing.* Ph.D. diss., Arizona State University.

Mack, L. M. 1984. Boundary-layer linear stability theory. In *Special Course on Stability and Transition of Laminar Flows*, AGARD R-709.

Malik, M. R., F. Li, and C. L. Chang. 1994. Crossflow disturbances in three-dimensional boundary layers: Nonlinear development, wave interaction and secondary instability. *J. Fluid Mech.* 268:1–36.

Mangalam, S. M., D. V. Maddalon, W. S. Saric, and N. K. Agarwal. 1990. Measurement of crossflow vortices, attachment-line flow, and transition using microthin hot films. AIAA Paper 90-1636.

Meyer, F. and L. Kleiser. 1990. Numerical simulation of transition due to crossflow instability. In *Laminar-Turbulent Transition* (eds. D. Arnal and R. Michel), vol. 3, pp. 609–619. Berlin: Springer-Verlag. ISBN 3-540-52196-8.

Müller, B. 1990. Experimental study of travelling waves in a three-dimensional boundary layer. In *Laminar-Turbulent Transition* (eds. D. Arnal and R. Michel), vol. 3, pp. 489–498. Berlin: Springer-Verlag. ISBN 3-540-52196-8.

Müller, B. and H. Bippes. 1989. Experimental study of instability modes in a three-dimensional boundary layer. In *Fluid Dynamics of Three-Dimensional Turbulent Shear Flows and Transition*, AGARD CP-438. Loughton, Essex: Specialised Printing Services Ltd. ISBN 92-835-0502-6.

Müller, B., H. Bippes, and F. S. Collier, Jr. 1990. The stability of a three dimensional boundary layer over a swept flat plate. In *Instability and Transition* (eds. M. Y. Hussaini and R. G. Voight), vol. 2, pp. 268–277. New York: Springer-Verlag. ISBN 0-387-97324-9.

Nitschke-Kowsky, P. and H. Bippes. 1988. Instability and transition of a three-dimensional boundary layer on a swept flat plate. *Phys. Fluids* 31(4):786–795.

Poll, D. I. A. 1979. Transition in the infinite swept attachment line boundary layer. *Aeronaut. Q.* 30:607–629.

Poll, D. I. A. 1984. Transition description and prediction in three-dimensional flows. In *Special Course on Stability and Transition of Laminar Flows*, AGARD R-709.

Poll, D. I. A. 1985. Some observations of the transition process on the windward face of a long yawed cylinder. *J. Fluid Mech.* 150:329–356.

Radeztsky, R. H. Jr., M. S. Reibert, W. S. Saric, and S. Takagi. 1993. Effect of micron-sized roughness on transition in swept-wing flows. AIAA Paper 93-0076.

Radeztsky, R. H. Jr., M. S. Reibert, and W. S. Saric. 1994. Development of stationary crossflow vortices on a swept wing. AIAA Paper 94-2373.

Reed, H. L. and R.-S. Lin. 1987. Stability of three-dimensional boundary layers. SAE Paper 87-1857.

Reed, H. L. and W. S. Saric. 1989. Stability of three-dimensional boundary layers. *Ann. Rev. Fluid Mech.* 21:235–284.

Reed, H. L., W. S. Saric, and D. Arnal. 1996. Linear stability theory applied to boundary layers. *Ann. Rev. Fluid Mech.* 28:389–428.

Reibert, M. S. 1996. *Nonlinear Stability, Saturation, and Transition in Crossflow-Dominated Boundary Layers*. Ph.D. diss., Arizona State University.

Reibert, M. S., W. S. Saric, R. B. Carrillo, Jr., and K. L. Chapman. 1995. Nonlinear stability, saturation, and transition in swept-wing flows. In *Transitional Boundary Layers in Aeronautics* (eds. R. A. W. M. Henkes and J. L. van Ingen), pp. 125–135, Amsterdam. North-Holland Press. ISBN 0-444-85812-1.

Reibert, M. S., W. S. Saric, R. B. Carrillo, Jr., and K. L. Chapman. 1996. Experiments in nonlinear saturation of stationary crossflow vortices in a swept-wing boundary layer. AIAA Paper 96-0184.

Reshotko, E. 1994. Boundary layer instability, transition and control. AIAA Paper 94-0001.

Saric, W. S. 1992a. The ASU transition research facility. AIAA Paper 92-3910.

Saric, W. S. 1992b. Laminar-turbulent transition: Fundamentals. In *Special Course on Skin Friction Drag Reduction*, AGARD R-786. Loughton, Essex: Specialised Printing Services Ltd. ISBN 92-835-0661-8.

Saric, W. S. 1994. Görtler vortices. *Ann. Rev. Fluid Mech.* 26:379–409.

Somers, D. M. and K. H. Horstmann. 1985. Design of a medium-speed natural-laminar-flow airfoil for commuter aircraft applications. *DFVLR-IB/29-85/26*.

von Doenhoff, A. E. and A. L. Braslow. 1961. The effect of distributed roughness on laminar flow. In *Boundary-Layer Control* (ed. Lachmann), vol. 2. Pergamon.

Wang, M., T. Herbert, and G. K. Stuckert. 1994. Crossflow-induced transition in compressible swept-wing flows. AIAA Paper 94-2374.

Wintergerste, T. and L. Kleiser. 1995. Direct Numerical Simulation of transition in a three-dimensional boundary layer. In *Transitional Boundary Layers in Aeronautics* (eds. R. A. W. M. Henkes and J. L. van Ingen), pp. 145–154, Amsterdam. North-Holland Press. ISBN 0-444-85812-1.
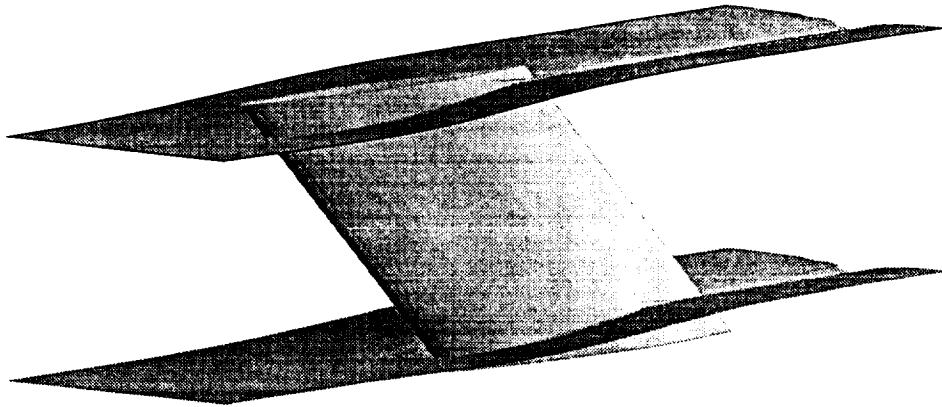
Figure 1: NLF(2)-0415 airfoil and wall liners removed from the Unsteady Wind Tunnel test section.
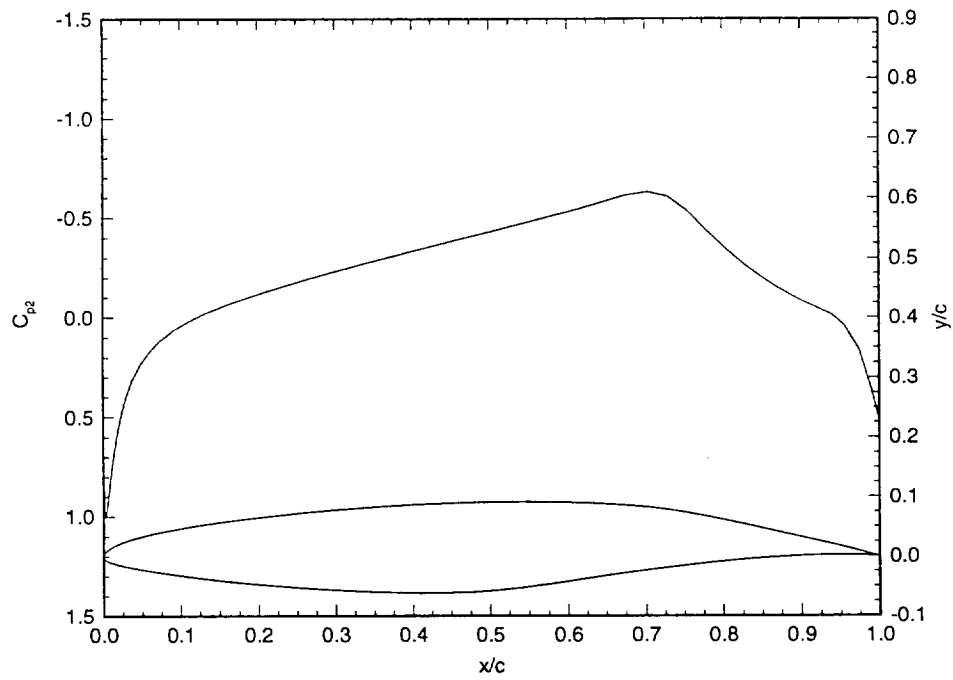
Figure 2: Unswept NLF(2)-0415 airfoil contour and theoretical upper-surface free-air C_p for $\alpha = -4°$. The C_p is computed with the NASA Langley code MCARF.
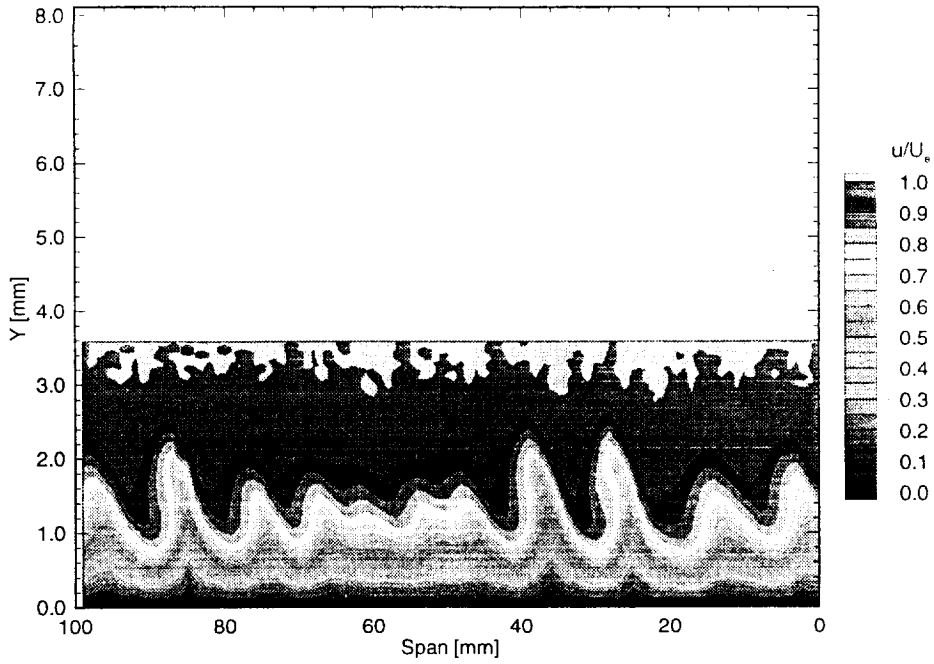
Figure 3: Streamwise velocity contours at $x/c = 0.45$, $Re_c = 3.0 \times 10^6$. No artificial roughness.
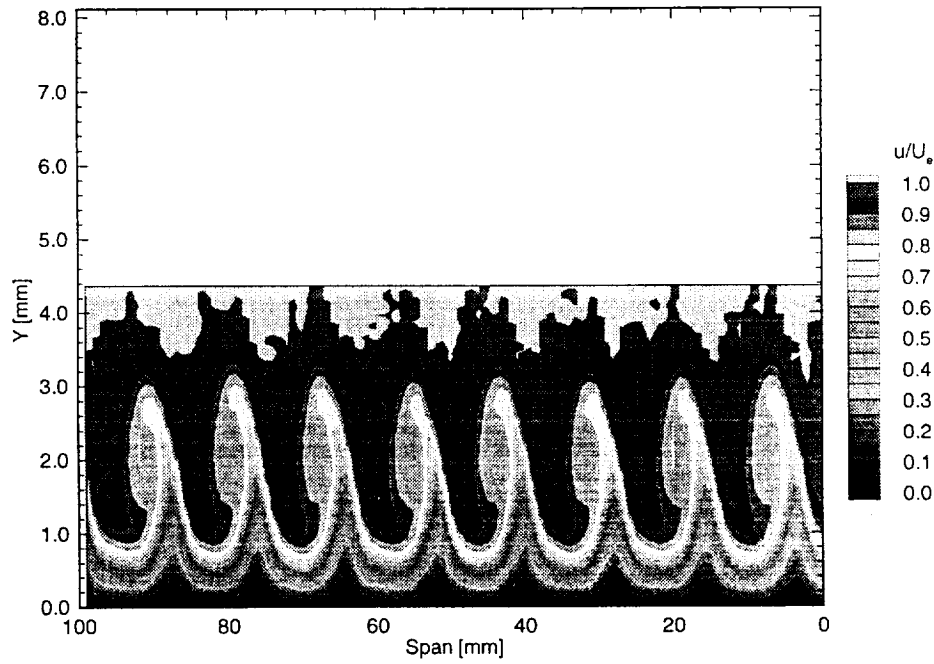
Figure 4: Streamwise velocity contours at $x/c = 0.45$, $Re_c = 2.4 \times 10^6$. A full-span array of $k = 6$ μm roughness elements with 12 mm spanwise spacing is at $x/c = 0.023$.
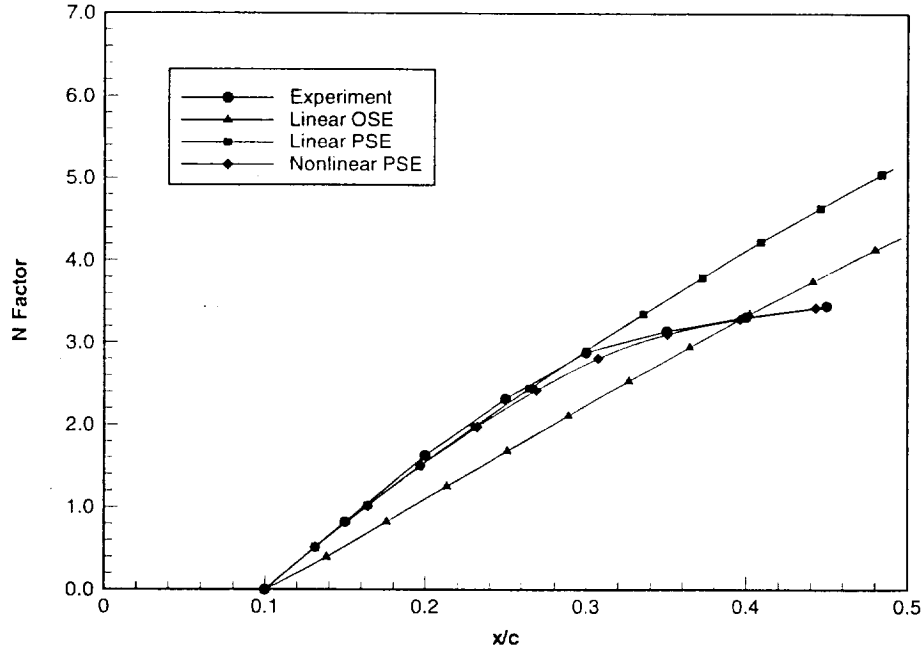
Figure 5: Measured and theoretical N-factors for the conditions of figure 4. All theoretical calculations include curvature.
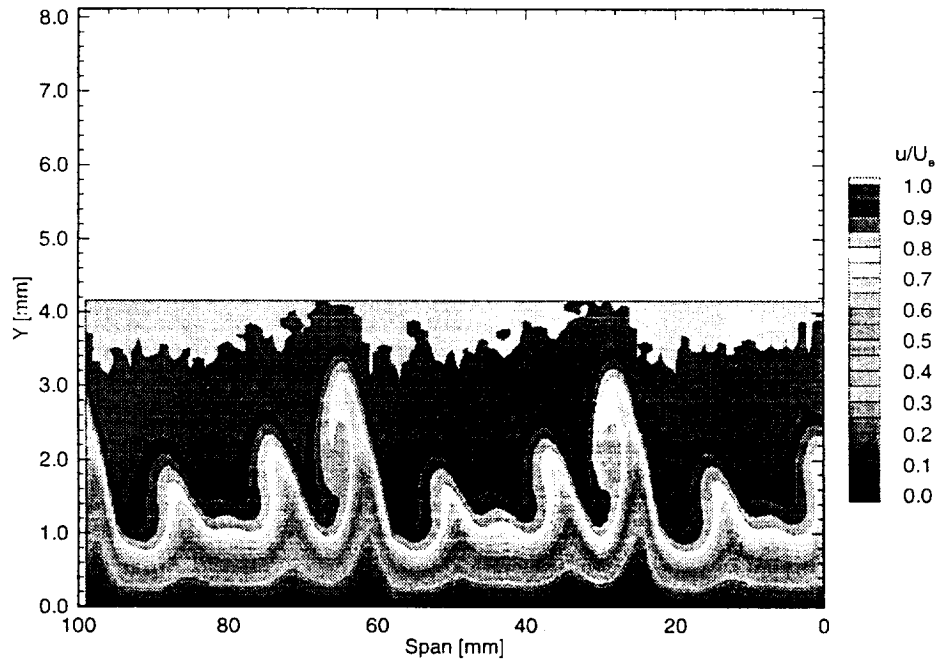
Figure 6: Streamwise velocity contours at $x/c = 0.45$, $Re_c = 2.4 \times 10^6$. A full-span array of $k = 6$ μm roughness elements with 36 mm spanwise spacing is at $x/c = 0.023$.
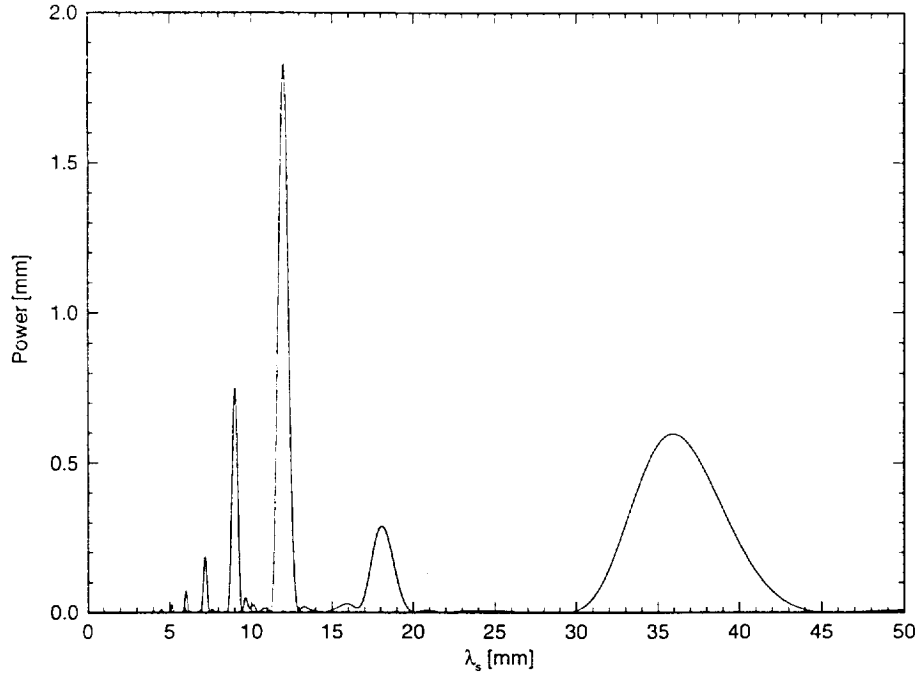
Figure 7: FFT-based power spectral density at $Y = 0.9$ mm for the conditions of figure 6.
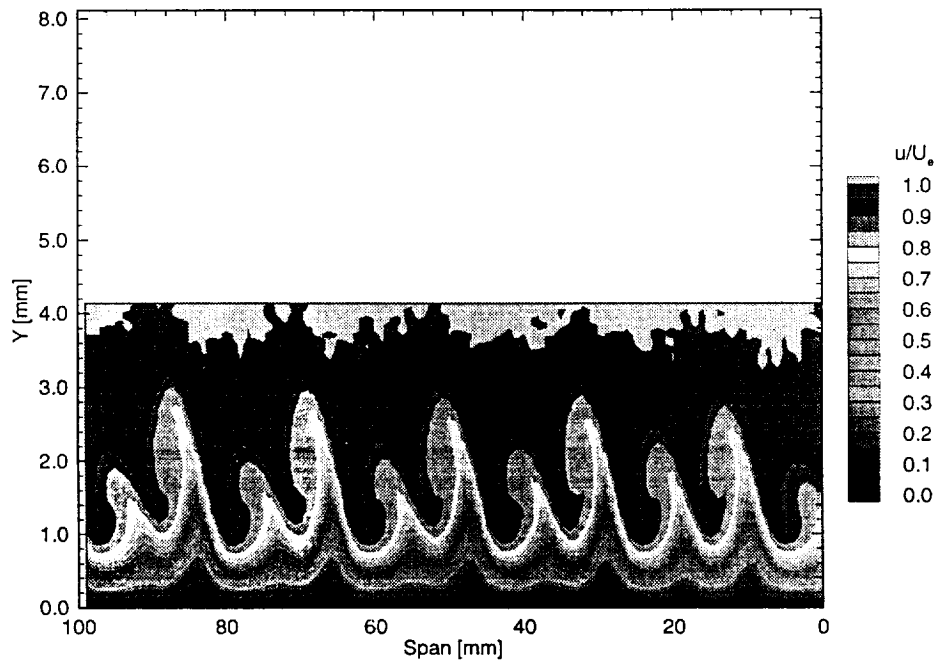
Figure 8: Streamwise velocity contours at $x/c = 0.45$, $Re_c = 2.4 \times 10^6$. A full-span array of $k = 6$ μm roughness elements with 18 mm spanwise spacing is at $x/c = 0.023$.
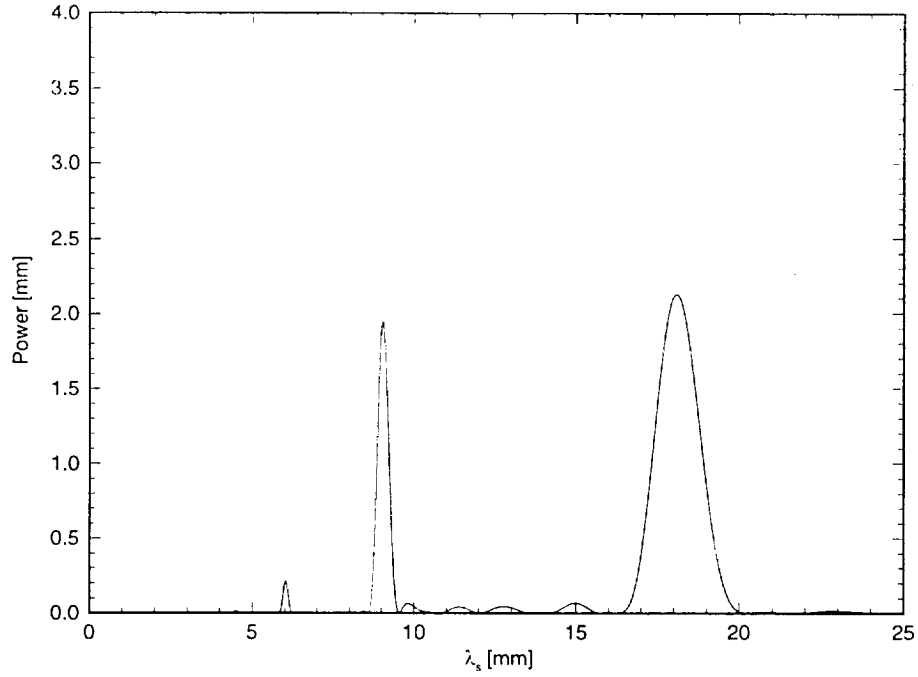
Figure 9: FFT-based power spectral density at $Y = 0.85$ mm for the conditions of figure 8.
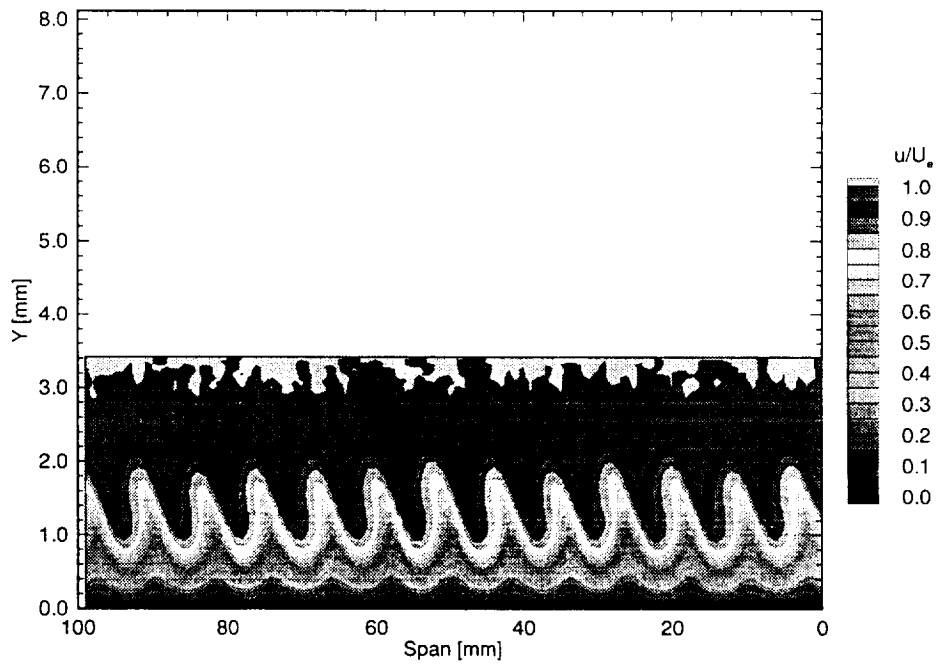
Figure 10: Streamwise velocity contours at $x/c = 0.30$, $Re_c = 2.4 \times 10^6$. A full-span array of $k = 6$ μm roughness elements with 8 mm spanwise spacing is at $x/c = 0.023$.

23
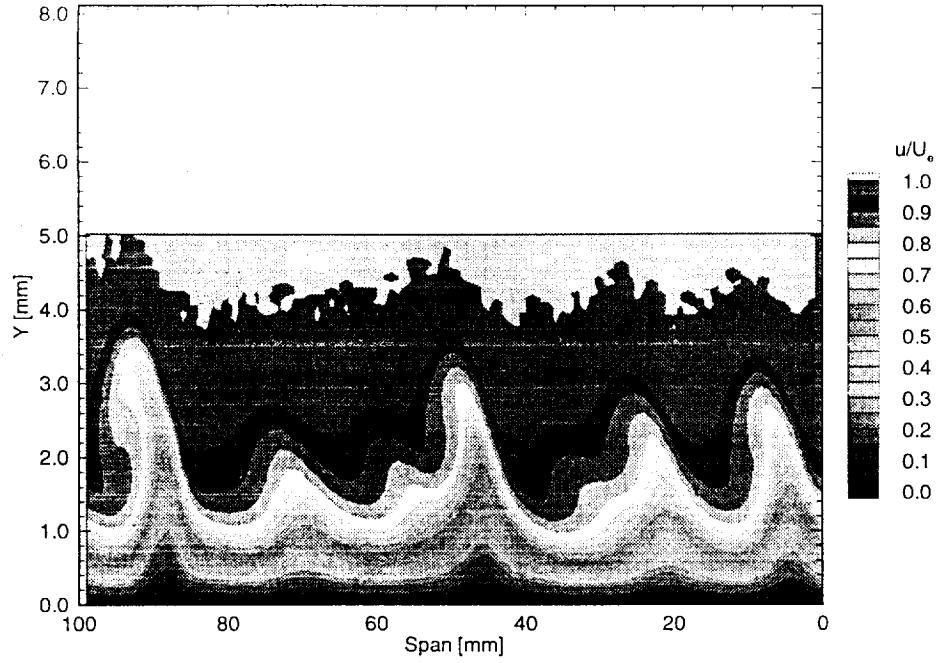
Figure 11: Streamwise velocity contours at $x/c = 0.60$, $Re_c = 2.4 \times 10^6$. A full-span array of $k = 6$ μm roughness elements with 8 mm spanwise spacing is at $x/c = 0.023$.
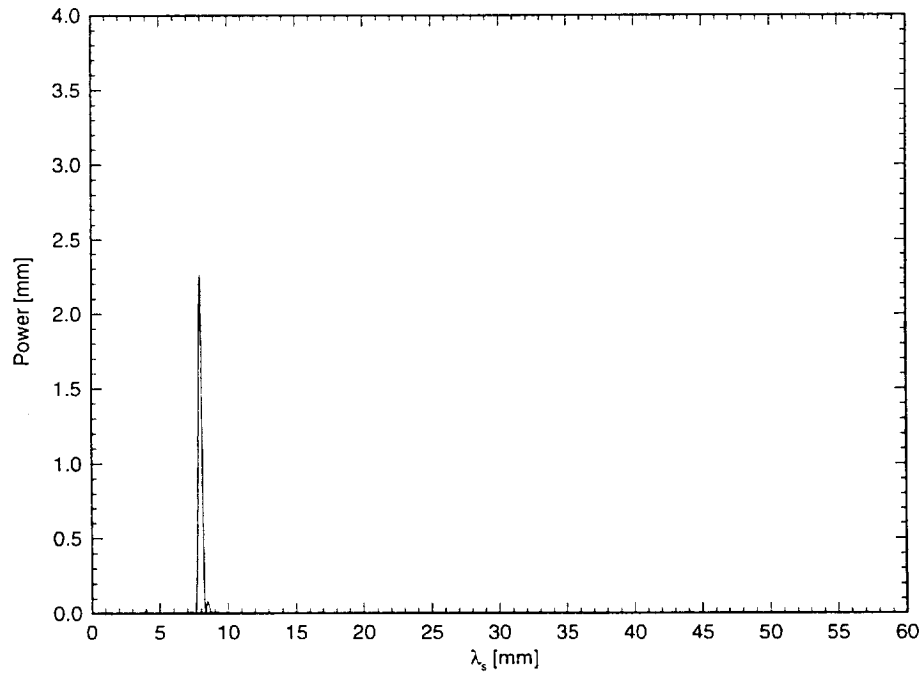
Figure 12: FFT power spectral density at $Y = 0.85$ mm for the conditions of figure 10.
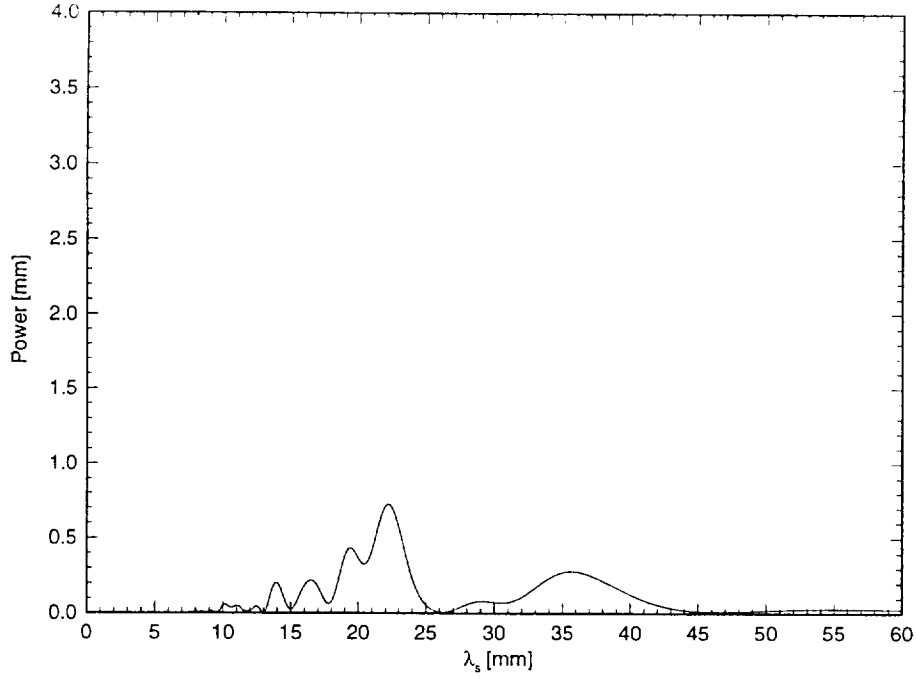
Figure 13: FFT power spectral density at $Y = 1.0$ mm for the conditions of figure 11.
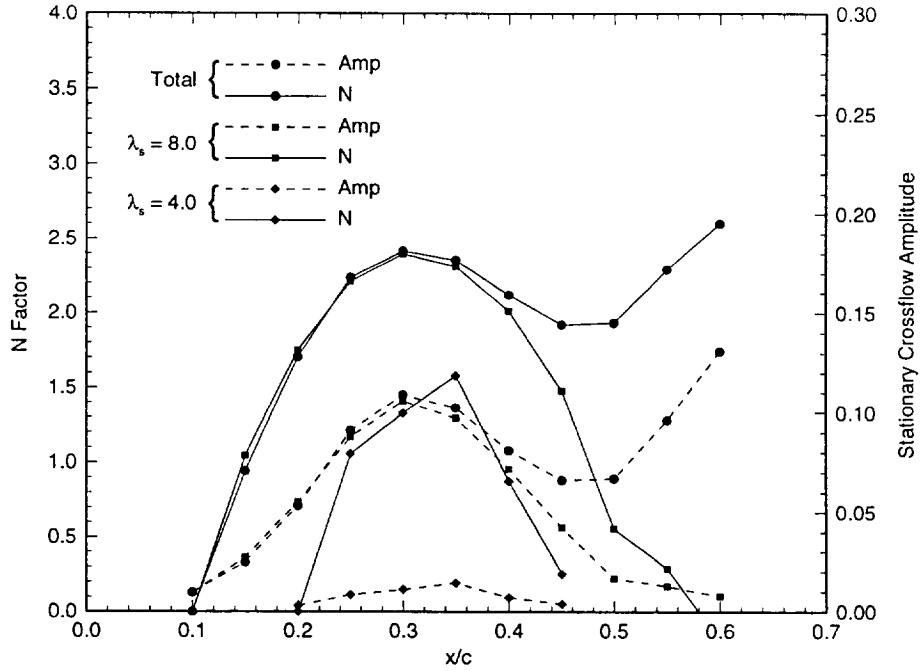
Figure 14: Total and single-mode disturbance amplitude and N-factors for $Re_c = 2.4 \times 10^6$. A full-span array of $k = 6$ μm roughness elements with 8 mm spanwise spacing is at $x/c = 0.023$. N-factor calculations are relative to the location where the disturbance is first detected.